ISSN 0010-9525, Cosmic Research, 2017, Vol. 55, No. 3, pp. 178–189. © Pleiades Publishing, Ltd., 2017.
Original Russian Text © Y.I. Yermolaev, I.G. Lodkina, N.S. Nikolaeva, M.Y. Yermolaev, M.O. Riazantseva, 2017, published in Kosmicheskie Issledovaniya, 2017, Vol. 55, No. 3, pp. 189–200.

Some Problems of Identifying Types of Large-Scale Solar Wind and Their Role in the Physics of the Magnetosphere

Y. I. Yermolaev*, I. G. Lodkina, N. S. Nikolaeva†, M. Y. Yermolaev, and M. O. Riazantseva

Space Research Institute of the Russian Academy of Sciences, Moscow, 117997 Russia

**e-mail: yermol@iki.rssi.ru*

Received August 15, 2016

Abstract—This paper discusses the errors in analyzing solar-terrestrial relationships, which result from either disregarding the types of interplanetary drivers in studying the magnetosphere response on their effect or from the incorrect identification of the type of these drivers. In particular, it has been shown that the absence of selection between the Sheath and ICME (the study of so-called *CME-induced storms*, i.e., magnetic storms generated by CME) leads to errors in the studies of interplanetary conditions of magnetic storm generation, because the statistical analysis has shown that, in the Sheath + ICME sequences, the largest number of storm onsets fell on the Sheath, and the largest number of storms maxima fell at the end of the Sheath and the beginning of the ICME. That is, the situation is observed most frequently when at least the larger part of the main phase of storm generation falls on the Sheath and, in reality, Sheath-induced storms are observed. In addition, we consider several cases in which magnetic storms were generated by corotating interaction regions, whereas the authors attribute them to CME.

DOI: 10.1134/S0010952517030029

1. INTRODUCTION

In the last decade, the investigations of solar-terrestrial relationships have gradually changed our ideas about the role of interplanetary drivers in generating the magnetospheric disturbances; whereas earlier, beginning with pioneer works [1–6], the main emphasis was placed on the behavior of the southward Bz component of the interplanetary magnetic field (IMF) and, to a lesser extent, to the density n and velocity V of solar wind, then, to date, a large experimental material is accumulated [7–28], which shows different magnetosphere response on various types of solar wind, even for close values of Bz, n, and V. That is, we see a more complicated and complex character of the dependence of magnetosphere response on various interplanetary medium parameters in the drivers of disturbances. This results in an increase in the number of investigations in which some magnetospheric, ionospheric, and atmospheric processes are compared with some particular types of solar wind. The participants of these investigations, who are not specialists in solar wind, have often used unverified sources of information on types of solar wind for the time intervals they needed, or they try to independently identify types of solar wind. In addition, in reality, it often ignored that some events in the solar wind represent a sequence of various types of solar wind, each of which can be a magnetospheric disturbance driver. For example, in reality, CME-induced magnetic storms can be generated by a Sheath, the coronal mass ejection (CME) body (an interplanetary coronal mass ejection (ICME), including the magnetic cloud (MC) or Ejecta) or by their sequence. This leads to the incorrect identification of types of solar wind and, as a consequence, to significant errors in data analysis and to incorrect conclusions. In this work, we will consider some examples that demonstrate these shortcomings.

2. TECHNIQUE

In this paper, we use the classification of types of solar wind, the choice of which was justified and described in our paper [29]. This classification was based on the ideas and experimental data on the solar-terrestrial physics available in the world literature and includes three types of quasi-stationary solar wind (fast and slow types of solar wind generated in the coronal holes and in the coronal streamer belts, respectively, as well as the heliospheric current sheet); six types of disturbed solar wind, including the compression region in front of the fast solar wind stream, i.e., the corotating interaction region (CIR); ICMEs, which include the magnetic clouds (MCs) and Ejecta; the compression regions of the Sheath in front of fast MCs and Ejecta (SH_{MC} and SH_{EJ}, respectively); and rarefaction regions behind the ICME (Rare), as well

† Deceased.

as forward and reverse interplanetary shocks IS and ISa. Based on 1-h data of the OMNI database (http://omniweb.gsfc.nasa.gov [30]), we produced a catalog of indicated solar wind phenomena for the 25-year interval of 1976–2000 [29], and this catalog continues to be expanded in the coverage time (ftp://ftp.iki.rssi.ru/pub/omni/). To analyze the magnetosphere response on the change of interplanetary conditions, we restricted ourselves to the following disturbed types of solar wind, i.e., CIR, two types of Sheath (SH_{MC} and SH_{EJ}), two types of ICMEs (MC and Ejecta), and IS forward shocks.

There are some works that describe the average values of plasma and magnetic field parameters in the indicated types of solar wind, which are in good agreement within statistical scattering (see, e.g., [31, 32] and references therein), which confirms the accepted classification with small variations in the identification techniques and distinctions in selected intervals. However, the average temporal profiles of parameters for particular types of solar winds are of particular interest. Because the durations of single-type phenomena may differ, we have applied the double-superposed-epoch-analysis method, which entails a proportional increase or decrease in the time step between the points such that the times of the beginnings and ends of the intervals coincide for all phenomena of the chosen type [23]. After the alignment of the edges of intervals, the durations of intervals of each type of solar wind were made equal to the average length of a corresponding type of solar wind, expressed in integer hours [26, 39]. Thus, we were able to obtain the temporal profiles of parameters of indicated types of solar wind. In order to take into account the real conditions of observations of various types of solar wind in the interplanetary space, including the interactions of these phenomena among themselves and with surrounding solar wind, we constructed the temporal profiles for eight different sequences of phenomena: (1) SW/CIR/SW, (2) SW/IS/CIR/SW, (3) SW/Ejecta/SW, (4) SW/Sheath/Ejecta/SW, (5) SW/IS/Sheath/Ejecta/SW, (6) SW/MC/SW, (7) SW/Sheath/MC/SW, and (8) SW/IS/Sheath/MC/SW, where SW is the undisturbed quasi-stationary solar wind [26]. On one hand, these average profiles allow one to explore various types of solar wind separately, as well as the presence and influence of adjacent types, as in the case when, in front of the body of coronal mass ejection ICME (separately for MC and Ejecta), Sheath compression regions and interplanetary shocks are observed. On the other hand, these average profiles of parameters can be used as a kind of templates in the identification of the chosen solar wind interval. Below, we use this comparison with templates to confirm the incorrect identification of the type of solar wind for some examples taken from the literature.

3. RESULTS

This section discusses the following two questions in detail: (1) the comparative Sheath and ICME contribution to the generation of magnetic storms in the study of CME-induced storms, and (2) the incorrect attribution of CIR intervals to cases of CME-induced storms.

3.1. Joint analysis of Sheath and ICME. The authors of some studies have compared the magnetosphere response to the CME- and CIR-driven magnetic storms. That is, in the first case, it was not taken into account that the CMEs observed near the Sun, in the Earth's orbit may form Sheath and IS in addition to the body of the CME itself (MC and Ejecta). In this case, they have studied Sheath + ICME complex events without separating them into Sheath and ICME, including events that, in some cases, contain the shock (see, e. g., papers [11, 16, 28, 33–38]. In particular, paper [11] indicates 21 distinctions for CIR- and CME-induced magnetic storms; however, the important question, i.e., with which types of solar wind (IS, Sheath, MC or Ejecta) particular properties and distinctions for the CME-induced magnetic storms are associated, remains open.

Figures 1 and 2 show the average temporal profiles of magnetospheric indices *Dst, Dst** (the pressure-corrected *Dst* index [5]), *Kp*, and *AE* for the following six different sequences of solar wind phenomena: (1) SW/Ejecta/SW, (2) SW/Sheath/Ejecta/SW, (3) SW/IS/Sheath/Ejecta/SW, (4) SW/MC/SW, (5) SW/Sheath/MC/SW, (6) SW/IS/Sheath/MC/SW obtained by the double superposed epoch method similarly to paper [26] we have combined the beginnings and ends of the Sheath, Ejecta, and MC intervals and made the durations close to the average values of 10 h for the Sheath and 25 h for the Ejecta/MC. It should be emphasized that, when constructing these drawings, we used all events of the indicated type for 1976–2000 from our catalog [29] (695 Ejecta, 451 CIRs, 402 Sheath and 60 MCs), but not only the phenomena that caused the magnetic storm.

The panels in the first and third rows of Fig. 1 show that, on average, the *Dst* and *Dst** indices, which mainly reflect the behavior of a ring current and the excitation of magnetic storms for MC and Ejecta without Sheath or IS, are constant during the phenomenon and are equal to −10 and −35 nT, respectively; here, *Dst* and *Dst** are close to each other. A higher variability of indices for MC is associated with scare phenomena statistics. For both ICME types (MC and Ejecta) with Sheath but without IS, the average behavior of indices is divided into two parts, i.e., (1) the drop in *Dst* and *Dst** indices is observed in the Sheath (with minima of −50 nT in the early hours in the MC and −35 nT in the Ejecta, respectively, and the *Dst** index is systematically 5–10 nT lower than *Dst*) and (2) the

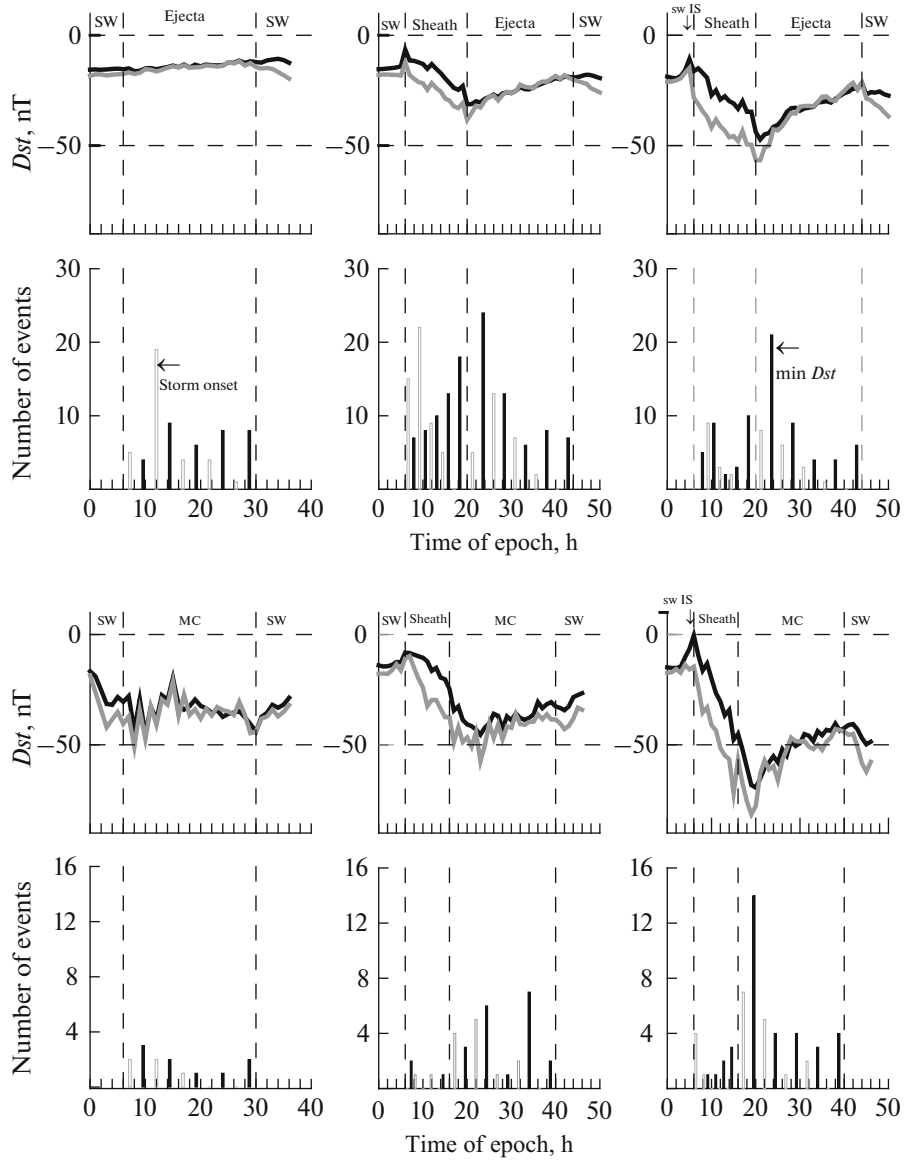

Fig. 1. Temporal profile of *Dst* (black) and *Dst** (gray) indices for six different sequences of solar wind phenomena. Vertical dashed lines indicate (from right to left): 1. last point of the Ejecta/MC intervals; 2. first point of the Ejecta/MC intervals; 3. (in the presence of Sheath) first point of the Sheath intervals. Panels of second and fourth rows show the distributions, in Sheath or Ejecta/MC time interval, number of beginnings of storms (light columns) and number of maxima (*Dst* index minima) of storms (black columns).

slight increase in *Dst* and *Dst** indices in the MC and Ejecta. For the MC and Ejecta with Sheath and IS, in general, the picture is identical for MC and Ejecta with Sheath and without IS, the only difference being that the *Dst* and *Dst** minima are –70 and –50 nT. The fact that the corrected *Dst** index in the Sheath is systematically lower than the measured *Dst* index is associated with higher values of density and pressure in the Sheath regions compared to the MC and Ejecta.

It should be emphasized that, on average, the duration of the main phase of the magnetic storm is about 7 h and the duration of the recovery phase (when the *Dst* index magnitude drops down to the level of $1/2\,|Dst_{\min}|$) is about 15 h [25], whereas the durations of Sheath, MC and Ejecta are, on average, about 15, 25, and 30 h [39]. Thus, Figs. 1 and 2, which include all events for 1976–2000, were obtained by averaging two types of events, i.e., (1) events in which the interplanetary phenomenon did not cause a magnetospheric disturbance, and (2) events in which short (compared to the duration of interplanetary phenomena) disturbances of the magnetosphere arose. In contrast to Figs. 1 and 2, the average temporal profiles of these disturbances for various types of solar wind

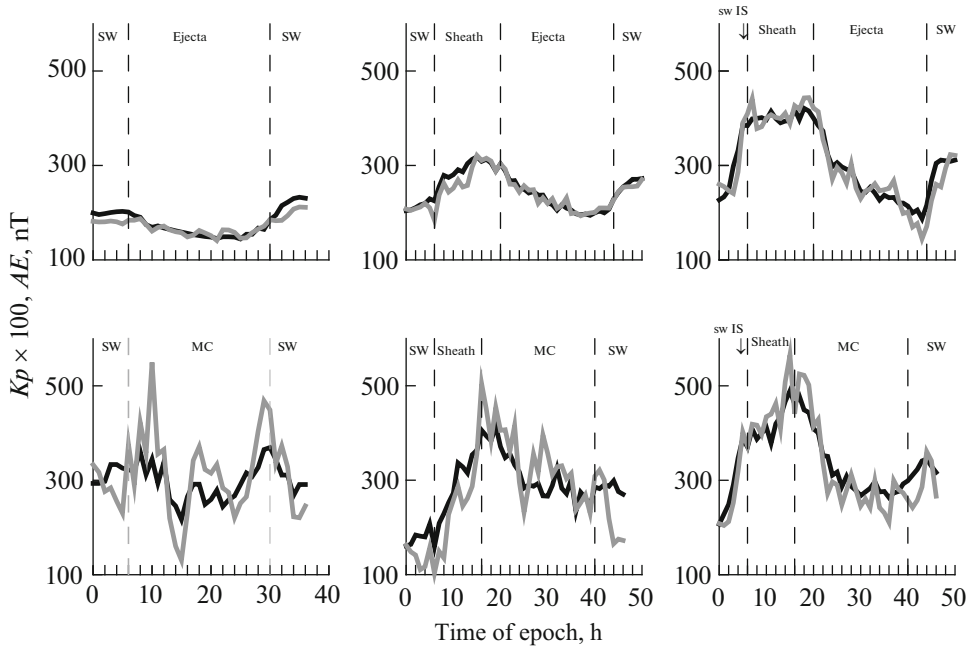

Fig. 2. Temporal profile of *Kp* (black) and *AE* (gray) indices for six different sequences of solar wind phenomena as in Fig. 1.

(145 magnetic storms generated by CIRs, 62 by MCs, 161 by Ejecta, 96 by Sheath), obtained by the of double superposed epoch method [23], are presented in Fig. 3. The average duration of the main phase of a magnetic storm is about 7 h.

In order to understand, in which manner the typical average temporal profiles of indices on the panels of the 1st and 3rd rows of Fig. 1 were obtained, we investigated the magnetic storms distribution in the length of Sheath and Ejecta/MC intervals. To this end, we divide the Sheath and Ejecta/MC intervals into five subintervals equal in time and counted the number of magnetic storms in each subinterval. The panels of the second and fourth rows of Fig. 1 show the time distributions for the Sheath and Ejecta/MC intervals, respectively, of the number of the following events: the onsets of storms with $Dst < -50$ nT (light columns) and the *Dst* minima (dark columns). Though the light and dark columns in the figure are shifted with respect to each other for clarity, they were calculated in the identical subintervals. These data show that a great number of magnetic storms began at the beginning of Sheath, and the maximum number of *Dst* index minima (the maxima of magnetic storms) fell at the end of Sheath to the beginning of Ejecta/MC.

For convenience of comparing the global *Kp* index and the auroral *AE* index, we multiplied the *Kp* index in Fig. 2 by 100. Both indices only slightly change for Ejecta without Sheath or IS and, for MC without Sheath or IS, the indices synchronously change within noticeable limits without an explicit trend (as in Fig. 1, this is due to the scarce statistics of events). On the remaining panels in Fig. 2, the indices behave similarly to Fig. 1: the appearance of the Sheath compression region in front of MC and Ejecta results in a situation where the activity grows during the Sheath (the indices increase nearly proportionally) and, during the MC and Ejecta the activity drops; here, the activity is higher for MC than for Ejecta, and it is higher for the events with the interplanetary shock IS than without it.

3.2. Incorrect identification of CIR. In this section, we will consider two examples in which the CIR phenomenon was identified as the ICME.

In paper [40], the authors have studied 143 CME- and CIR-driven storms in 1997–2008 and, to identify the types of interplanetary drivers, they have used the following criteria: "A CME signature is characterized as having simultaneous increases in the velocity of solar wind, pressure, proton density and ion temperature, compared to a CIR signature that first has peaks in the pressure and density of the solar wind, followed by subsequent rises in the velocity of solar wind and temperature during decreasing pressure and density." Note that the above criteria for CIR qualitatively correspond to the generally accepted definition of CIR, but the criteria for CME do not absolutely correspond to the generally accepted definition of the CME body, in which the decrease of the temperature and density (and, therefore, of the pressure) should be observed. Perhaps the authors had in mind the compression region in front of the CME, i.e., the Sheath, but this statement was not mentioned anywhere in the text.

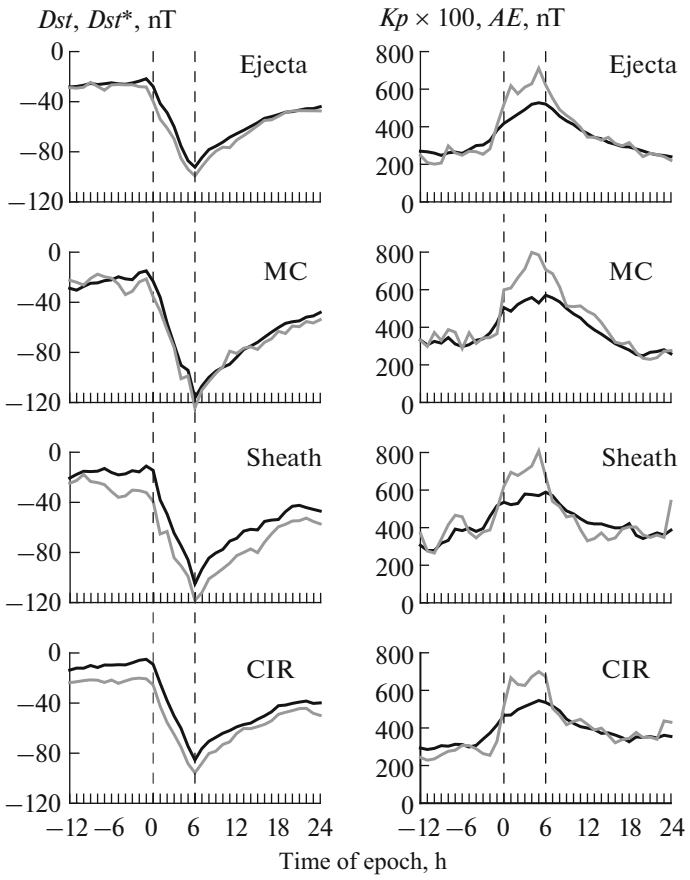

Fig. 3. Time dependence of *Dst*, *Dst** (left panels; black and gray lines), *Kp*, and *AE* (right panels; black and gray lines) indices for magnetic storms. Vertical lines indicate the first and last points of the main phase of magnetic storms.

As an example of a typical CME, Figure 2a in paper [40] presents the temporal profiles of some parameters of solar wind's plasma and magnetic field for April 6–7, 2000, which have led to the magnetic storm excitation. The caption to this figure states, "A typical coronal mass ejection trace seen in ACE OMNI data with simultaneous increases in all components, i.e., the magnitude of interplanetary magnetic field, the velocity, pressure, density, and temperature of the solar wind." The analysis of this interval indicates that the compression region with a shock is observed here and, because this region is followed by a high-velocity solar wind stream, rather than by the ICME, this compression region represents the CIR (see the catalog of solar wind phenomena at <ftp://www.iki.rssi.ru/pub/omni> and paper [29]).

Figures 4 and 5 present the following data: gray lines represent the average temporal profiles of some parameters obtained by the double superposed epoch method for the SW/IS/CIR/SW sequence of phenomena [26]; black lines present the same parameters measured (the OMNI2 database) in the interval since 16.00 UT on April 6, 2000 to 8.00 UT on April 7, 2000. The figures present the following parameters:

Fig. 4. (a) proton temperature *T*; (b) density *N*; (c, d, e) the value of bulk velocity *V* and two angles are latitudinal (ϑ) and longitudinal (ϕ); (f, g) Alfvén and sound velocities *Va* and *Vs*; (h) thermal pressure *Pt*; (*i*) ratio of measured temperature to that estimated from the average relation between temperature and velocity of solar wind *T*/*T*exp; (j) and the ratio of thermal and magnetic pressures β.

Fig. 5. (a, b, c, d) magnitude of *B* and *Bx*; *By, Bz* are components of the interplanetary magnetic field; (e) convective electric field $Ey = VBz$; (f) dynamic pressure *Pd*; (g, h, i, j) magnetospheric indices *AE, Kp, Dst*,* and *Dst*.

The main distinction of this phenomenon from the average picture for the CIR with IS, which was obtained in paper [26], is the great difference between the velocities in the high-velocity stream (about 620 km/s) and the slow stream (about 380 km/s); i.e., the difference between velocities in the fast and slow solar-wind streams was about 240 km/s, whereas, on average, it equals about 100 km/s. First of all, this caused a high

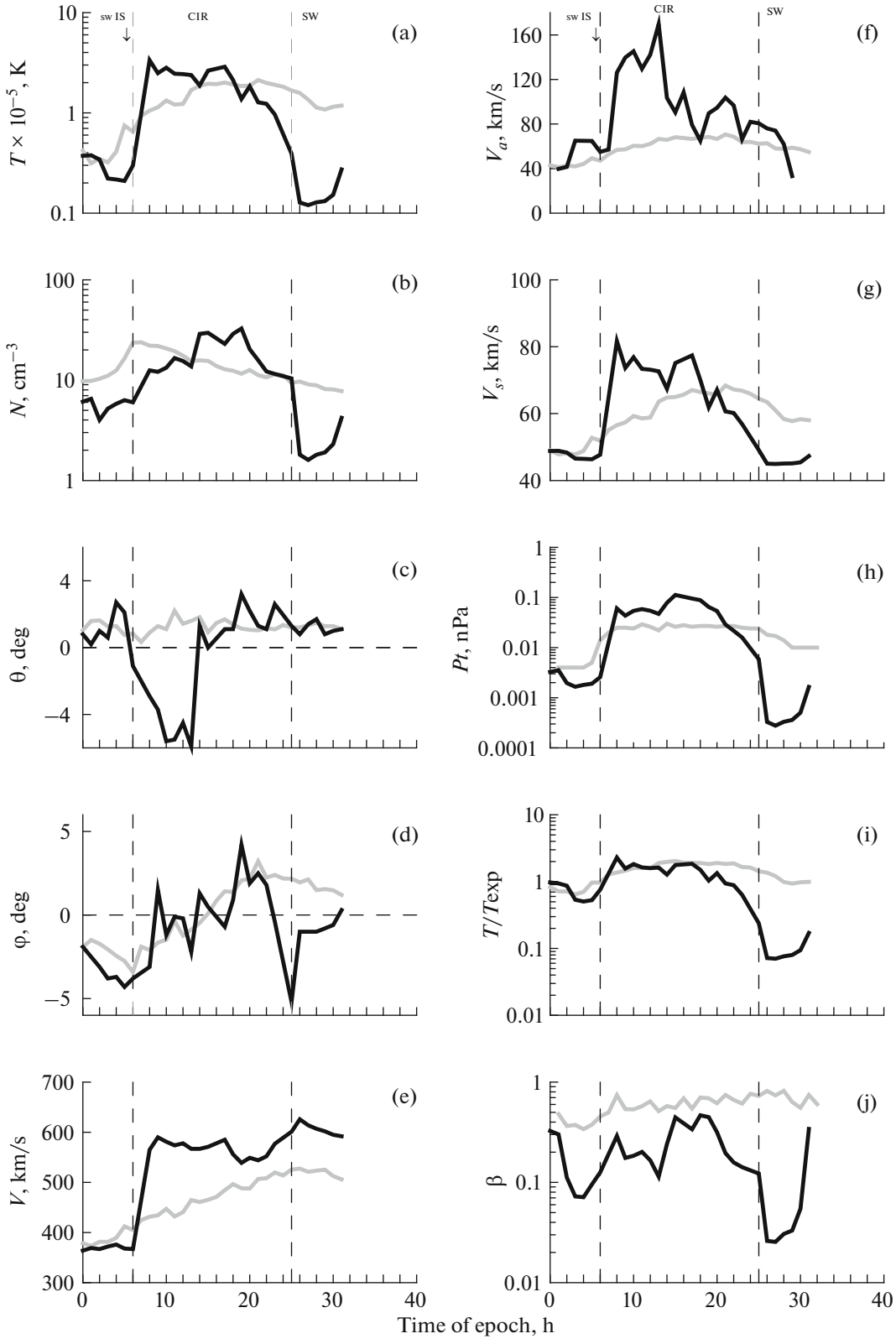

Fig. 4. Average temporal profiles of interplanetary medium parameters and magnetospheric indices, obtained by the double superposed epoch method for SW/IS/CIR/SW sequence of phenomena (gray lines) and the same parameters measured (OMNI2 database) at 16.00 UT on April 6, 2000 to 8.00 UT on April 7, 2000 (black lines).

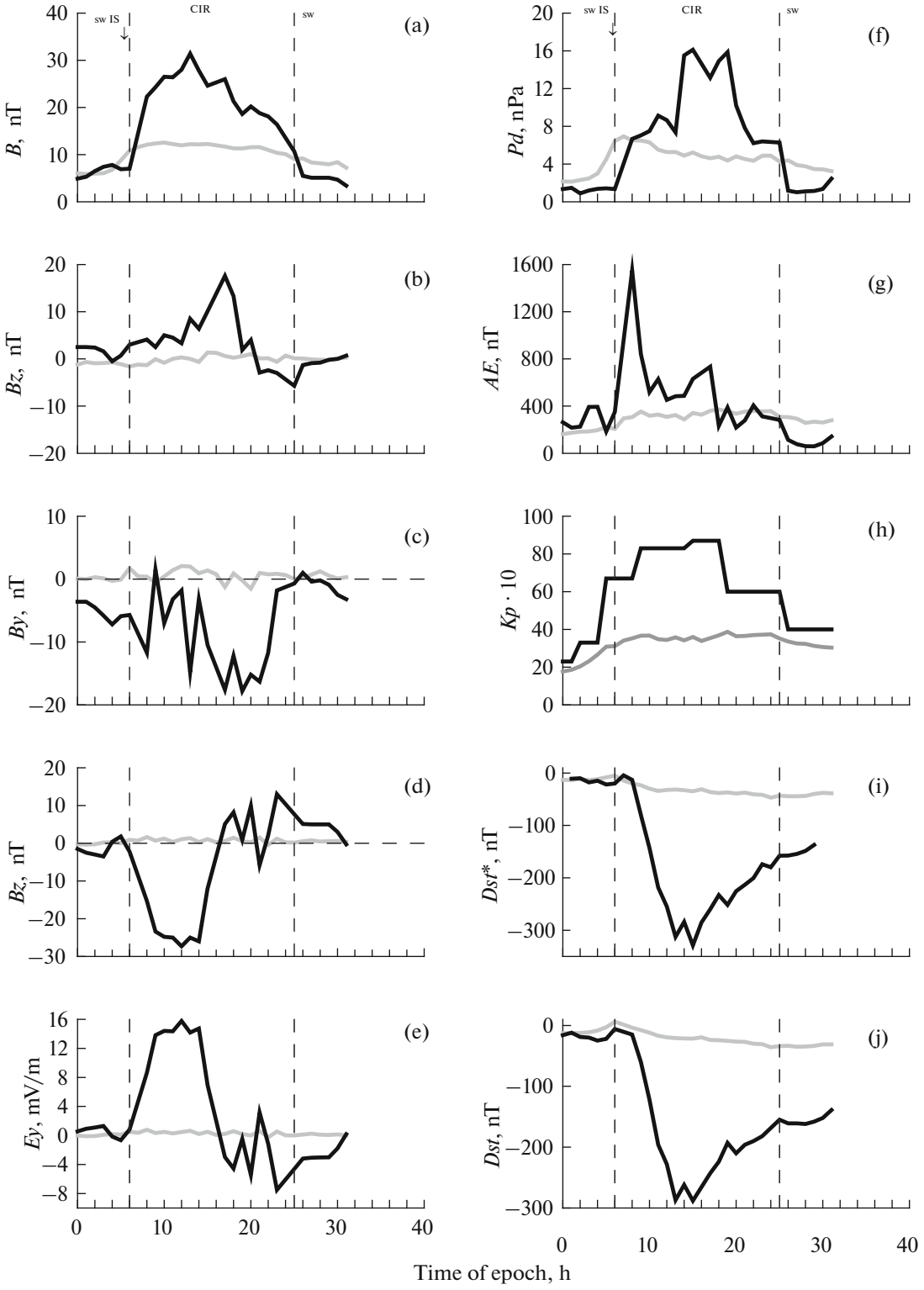

Fig. 5. Continuation of Fig. 4.

increase in the magnitude and components of the magnetic field and related parameters (the Alfvén velocity, β parameter), as well as of the dynamic pressure. Nevertheless, the basic parameters that characterize the compression region (temperature, density, temporal profile and rotation in the angle φ in the ecliptic plane, velocities, the ratio of temperatures T/Texp, thermal pressure) are in well agreement with

the average dynamics of parameters. This quantitatively confirms that the given interval relates to the CIR type.

At the beginning of this interval, the formation of the large, long-lasting *Bz* component of the IMF (its formation coincides in time with a strong turning of a stream under the ecliptic plane, observed from the angle θ of the bulk velocity of a stream) has led to a high magnetospheric activity manifested in all magnetospheric indices.

Thus, Figures 2a and 2b of paper [40] show two CIR events with the only difference that, in the first case, at the frontal edge of the CIR there exists the powerful interplanetary shock, which led to a drastic increase of velocity, temperature, density and IMF magnitude at the very beginning of the interval, whereas in the second case such a shock is absent, and the growth of the same parameters occurs, first, as a weak jump at the CIR boundary; then, more slowly throughout the CIR interval (with some break inside the CIR interval, which requires a more detailed study, than it is possible within the framework of this work).

In paper [41], the authors investigated magnetospheric-ionospheric disturbances for the interval of March 7–11, 2012. For this interval, the authors indicated a series of interplanetary shocks, all of which, in authors' opinion, were excited by various ICMEs. In particular, they associated the shock at ~3.00 UT on March 7, 2012 with the ICME. The data analysis carried out similar to the analysis of the interval of April 6–7, 2000 described above has shown that, behind the shock, the compression region was observed in front of a high-speed stream (in this case, as in the previous one, the ICME is absent because, prior to the next shock, one could observe the *T*/Texp*, N,* β parameters, and the IMF magnitude, which have the same values as in the undisturbed solar wind, and one could not see any rotation of the magnetic field from variations in its components); that is, a typical CIR with IS was observed here.

Figures 6 and 7 are similar to Figs. 4 and 5 and only differ from them in the fact that, instead of the OMNI2 database for the interval of 16.00 UT of April 6, 2000 to 8.00 UT of April 7, 2000, they present corresponding data for the interval of 04.00–18.00 UT of March 7, 2012. As for the previous interval, the values and temporal profiles of basic interplanetary parameters well agree with their average dynamics (taking into account the formation of high values of the IMF magnitude and components and corresponding change of field-related parameters) for the phenomenon of CIR with IS.

4. DISCUSSION AND CONCLUSIONS

As is shown in [26], the magnetic field in the Sheath is, on average, higher than in the Ejecta, and is close to the field value in the MC. In some cases, the field in the Sheath can grow by five to six times compared to the field value in the undisturbed solar wind stream before the Sheath [42]. Although the probability of the situation where the field in the Sheath will have a noticeable and long-lasting southward component required for magnetic storm generation will be slightly lower than in the MC and Ejecta [24], the Sheath possesses a higher efficiency of magnetic storm generation; for the same integral of electric field *Ey* in the solar wind, the Sheath excites storms that are roughly 50% stronger than the MC and Ejecta [18, 19]. It was shown in paper [26] that, on average, the *Dst* and *Dst** indices decreased in the Sheath (the corrected index decreases faster due to high pressure in the Sheath) and reached their minimum at the end of Sheath or at the very beginning of MC and Ejecta; furthermore, in the MC and Ejecta, they grew. In this work, we have shown that the maximum of the distribution of a number of storm maxima (minima of *Dst* indices) has fallen on the end of the Sheath and beginning of the MC and Ejecta, this distribution of storms maxima was mainly associated with the observed average temporal profiles of indices in the Sheath + MC/Ejecta phenomena sequence. It should be noted that, taking into account the well-known temporal asymmetry of magnetic storms (fast growth in the main phase of the storm and slow decrease in the recovery phase), at a uniform distribution of storm maxima in the combined Sheath + MC/Ejecta interval, the profile would have a descending character over the whole interval common to two types, which is not consistent with observations.

The presented data indicate that the CME-induced disturbances of the magnetosphere can represent the response to absolutely different interplanetary drivers or their successive impact. These drivers have different physical natures, possess different efficiencies of the impact on the magnetosphere and may lead to the implementation of different mechanisms of this impact. For example, we have recently shown [19–21] that, with a similar interplanetary impact (the identical integral of the convective electric field of the solar wind $Ey = V \cdot Bz$ [5]), the compression regions Sheath and CIR excited magnetic storms that were ~1.5 times stronger on average than the CME bodies (ICME) themselves. The study of CME-induced disturbances of the magnetosphere without selection of the types of drivers possesses the following disadvantages:

1. It is impossible to reveal the key physical relationships between the interplanetary conditions characteristic of various drivers and the state of the magnetosphere, and to understand which mechanisms of magnetospheric disturbance are implemented under the effect of various drivers.

2. It is impossible to construct quantitative models of the magnetospheric response to the impact of vari-

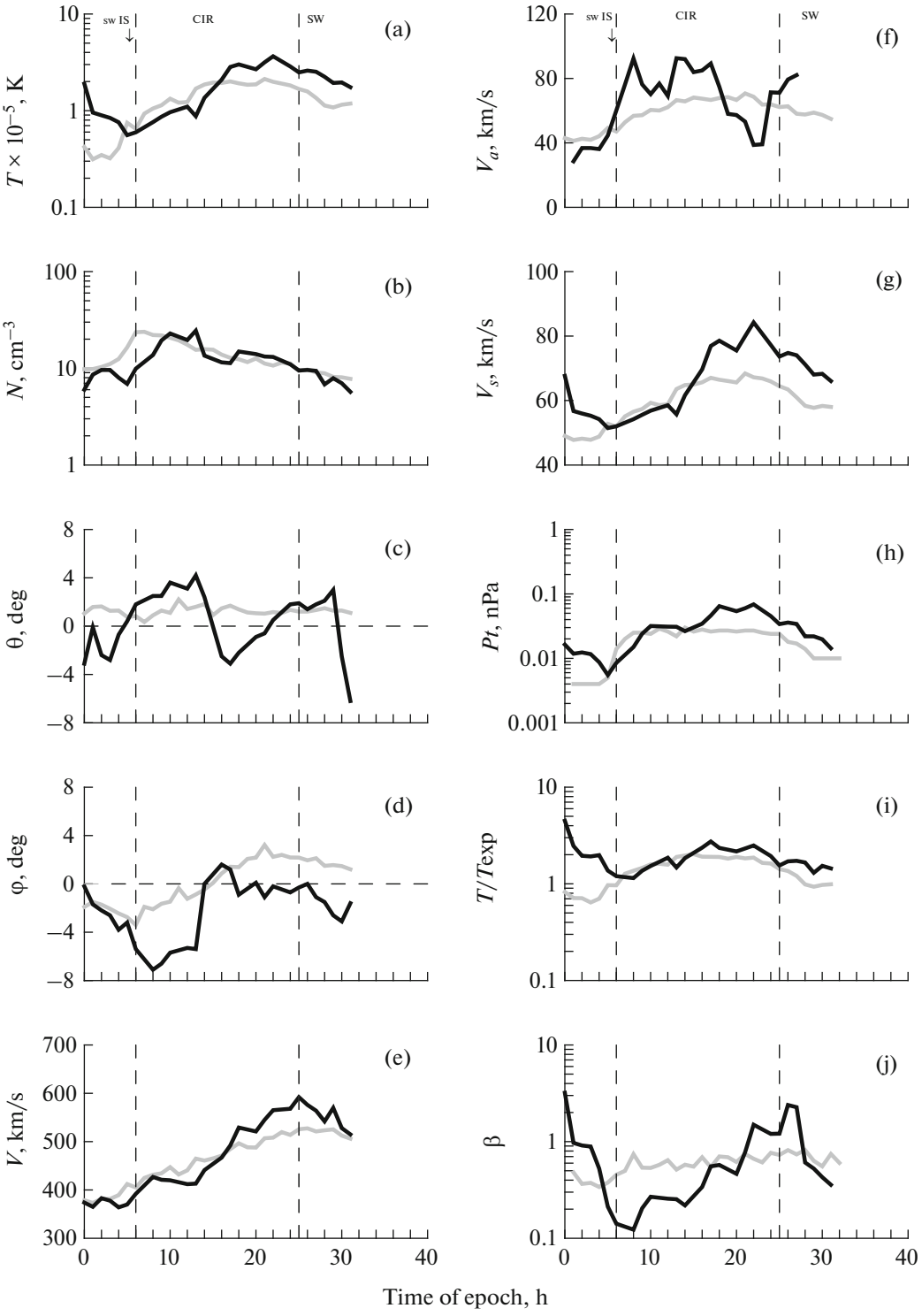

Fig. 6. Same as in Fig. 4 for 04.00–18.00 on March 7, 2012.

ous interplanetary drivers and to more correctly predict space weather.

The errors in identifying types of solar wind (types of interplanetary drivers) lead to the incorrect interpretation of the data and, ultimately, to erroneous conclusions. The examples of such kind of errors, presented in this work, indicate that they can often occur and, in connection with growing interest from researchers in identifying the types of solar wind in various disciplines, require taking measures to minimize this kind

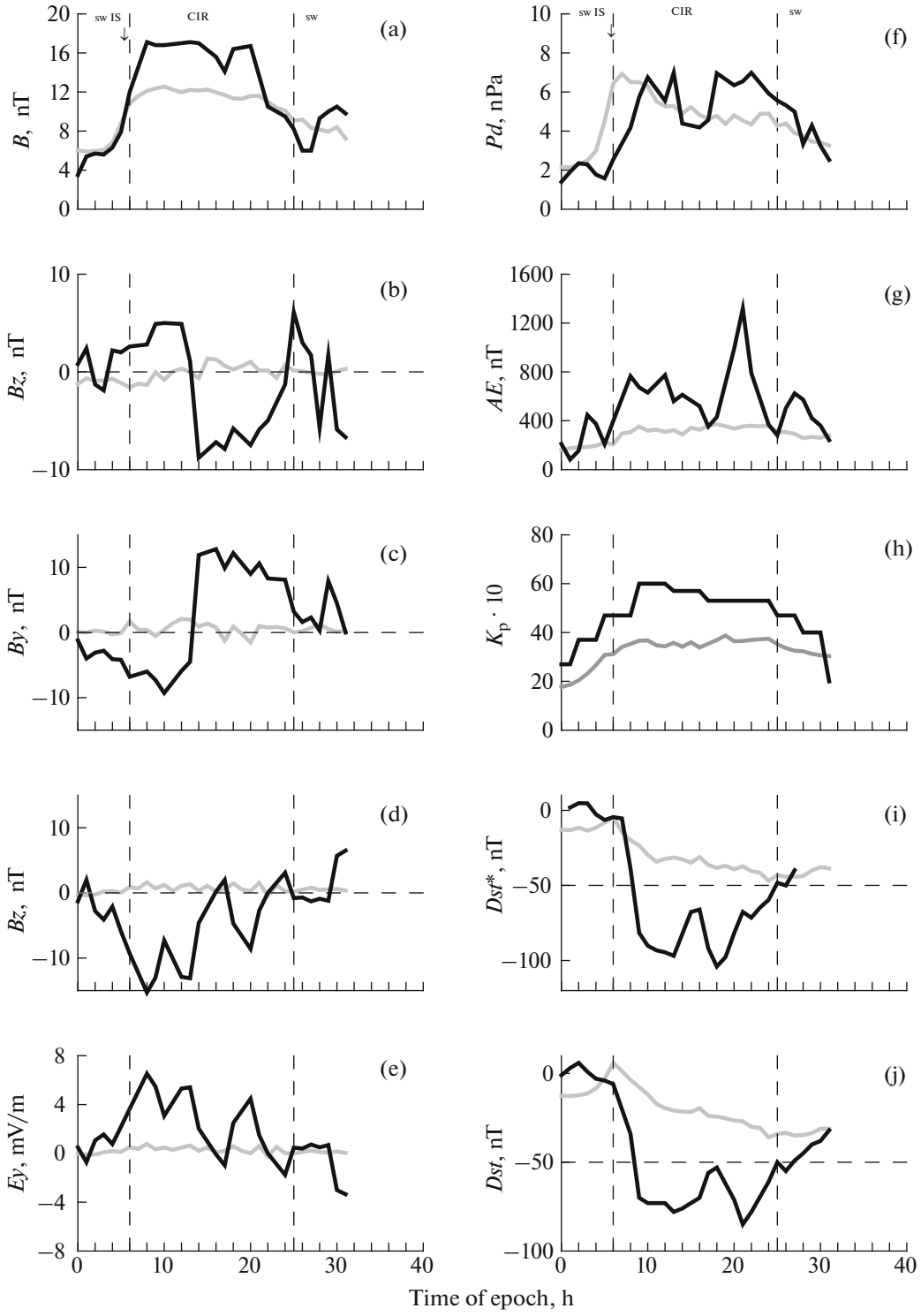

Fig. 7. Same as in Fig. 5 for 04.00–18.00 on March 7, 2012.

of error. One of these approaches could lie in the composition of the catalogs of types of solar wind by an international team of experts. These catalogs should be freely available and could be used by all stakeholders.

ACKNOWLEDGMENTS

The authors express their gratitude to the developers of the OMNI database (http://omniweb.gsfc.nasa.gov) for the opportunity to use it in the work. This work was

supported by Russian Science Foundation, project no. 16-12-10062.

REFERENCES

1. Dungey, J.W., Interplanetary magnetic field and the auroral zones, *Phys. Rev. Lett.*, 1961, vol. 6, no. 2, pp. 47–48.
2. Fairfield, D.H. and Cahill, L.J., The transition region magnetic field and polar magnetic disturbances, *J. Geophys. Res.*, 1966, vol. 71, pp. 155–169.
3. Rostoker, G. and Falthammar, C.-G., Relationship between changes in the interplanetary magnetic field and variations in the magnetic field at the Earth's surface, *J. Geophys. Res.*, 1967, vol. 72, no. 23, pp. 5853–5863.
4. Russell, C.T., McPherron, R.L., and Burton, R.K., On the cause of magnetic storms, *J. Geophys. Res.*, 1974, vol. 79, pp. 1105–1109.
5. Burton, R.K., McPherron, R.L., and Russell, C.T., An empirical relationship between interplanetary conditions and D_{st}, *J. Geophys. Res.*, 1975, vol. 80, pp. 4204–4214.
6. Akasofu, S.-I., Energy coupling between the solar wind and the magnetosphere, *Space Sci. Rev.*, 1981, vol. 111, A07S08. doi 10.1029/2005JA011447
7. Eselevich, V.G. and Fainshtein, V.G., An investigation of the relationship between the magnetic storm *Dst* indexes and different types of solar wind streams, *Ann. Geophys.*, 1993, vol. 11, no. 8, pp. 678–684.
8. Huttunen, K.E.J., Koskinen, H.E.J., and Schwenn, R., Variability of magnetospheric storms driven by different solar wind perturbations, *J. Geophys. Res.*, 2002, vol. 107, no. A7. doi 10.1029/2001JA900171
9. Huttunen, K.E.J. and Koskinen, H.E.J., Importance of post-shock streams and sheath region as drivers of intense magnetospheric storms and high-latitude activity, *Ann. Geophys.*, 2004, vol. 22, pp. 1729–1738.
10. Huttunen, K.E.J., Koskinen, H.E.J., Karinen, A., and Mursula, K., Asymmetric development of magnetospheric storms during magnetic clouds and sheath regions, *Geophys. Res. Lett.*, 2006, vol. 33, no. 6, L06107. doi 10.1029/2005GL024894
11. Borovsky, J.E. and Denton, M.H., Differences between CME-driven storms and CIR-driven storms, *J. Geophys. Res.*, 2006, vol. 28, pp. 121–190.
12. Pulkkinen, T.I., Partamies, N., Huttunen, K.E.J., Reeves, G.D., and Koskinen, H.E.J., Differences in geomagnetic storms driven by magnetic clouds and ICME sheath regions, *Geophys. Res. Lett.*, 2007, vol. 34, L02105. doi 10.1029/2006GL027775
13. Yermolaev, Yu.I., Yermolaev, M.Yu., Nikolaeva, N.S., and Lodkina, L.G., Interplanetary conditions for CIR-induced and MC induced geomagnetic storms, *Bulg. J. Phys.*, 2007, vol. 34, pp. 128–135.
14. Plotnikov, I.Y. and Barkova, E.S., Nonlinear dependence of *Dst* and *AE* indices on the electric field of magnetic clouds, *Adv. Space Res.*, 2007, vol. 40, pp. 1858–1862.
15. Longden, N., Denton, M.H., and Honary, F., Particle precipitation during ICME-driven and CIR-driven geomagnetic storms, *J. Geophys. Res.*, 2008, vol. 113, A06205. doi 10.1029/2007JA012752
16. Turner, N.E., Cramer, W.D., Earles, S.K., and Emery, B.A., Geoefficiency and energy partitioning in CIR-driven and CME-driven storms, *J. Atmos. Sol.-Terr. Phys.*, 2009, vol. 71, pp. 1023–1031.
17. Guo, J., Feng, X., Emery, B.A., et al., Energy transfer during intense geomagnetic storms driven by interplanetary coronal mass ejections and their sheath regions, *J. Geophys. Res.*, 2011, vol. 116, A05106. doi 10.1029/2011JA016490
18. Nikolaeva, N.S., Yermolaev, Yu.I., and Lodkina, I.G., Modeling the time behavior of the D_{st} index during the main phase of magnetic storms generated by various types of solar wind, *Cosmic Res.*, 2013, vol. 51, no. 6, pp. 401–412.
19. Nikolaeva, N.S., Yermolaev, Yu.I., and Lodkina, I.G., Dependence of geomagnetic activity during magnetic storms on solar-wind parameters for different types of streams: 4. Simulation for magnetic clouds, *Geomagn. Aeron. (Engl. Transl.)*, 2014, vol. 54, no. 2, pp. 152–161.
20. Nikolaeva, N., Yermolaev, Y., and Lodkina, I., Predicted dependence of the cross polar cap potential saturation on the type of solar wind stream, *Adv. Space Res.*, 2015, vol. 56, pp. 1366–1373.
21. Nikolaeva, N.S., Yermolaev, Yu.I., and Lodkina, I.G., Modeling of the corrected *Dst** index temporal profile on the main phase of the magnetic storms generated by different types of solar wind, *Cosmic Res.*, 2015, vol. 53, no. 2, pp. 119–127.
22. Yermolaev, Yu.I., Nikolaeva, N.S., Lodkina, I.G., and Yermolaev, M.Yu., Relative occurrence rate and geoeffectiveness of large-scale types of the solar wind *Cosmic Res.*, 2010, vol. 48, no. 1, pp. 1–30.
23. Yermolaev, Y.I., Nikolaeva, N.S., Lodkina, I.G., and Yermolaev, M.Y., Specific interplanetary conditions for CIR-induced, sheath-induced, and ICME-induced geomagnetic storms obtained by double superposed epoch analysis, *Ann. Geophys.*, 2010, vol. 28, pp. 2177–2186.
24. Yermolaev, Y.I., Nikolaeva, N.S., Lodkina, I.G., and Yermolaev, M.Y., Geoeffectiveness and efficiency of CIR, sheath, and ICME in generation of magnetic storms, *J. Geophys. Res.*, 2012, vol. 117, A00L07. doi 10.1029/2011JA017139
25. Yermolaev, Y.I., Lodkina, I.G., Nikolaeva, N.S., and Yermolaev, M.Y., Influence of the interplanetary driver type on the durations of the main and recovery phases of magnetic storms, *J. Geophys. Res.*, 2014, vol. 119, no. 10, pp. 8126–8136. doi 10.1002/2014JA019826
26. Yermolaev, Y.I., Lodkina, I.G., Nikolaeva, N.S., and Yermolaev, M.Y., Dynamics of large-scale solar wind streams obtained by the double superposed epoch analysis, *J. Geophys. Res.*, 2015, vol. 120, no. 9, pp. 7094–7106. doi 10.1002/2015JA021274
27. Borovsky, J.E., Cayton, T.E., Denton, M.H., Belian, R.D., Christensen, R.A., and Ingraham, J.C., The proton and electron radiation belts at geosynchronous orbit: Statistics and behavior during high-speed stream-driven storms, *J. Geophys. Res.*, 2016, vol. 121, no. 6, pp. 5449–5488. doi 10.1002/2016JA022520

28. Lockwood, M., Owens, M.J., Barnard, L.A., et al., On the origins and timescales of geoeffective IMF, *Space Weather*, 2016, vol. 14, pp. 406–432. doi 10.1002/2016SW001375

29. Yermolaev, Yu.I., Nikolaeva, N.S., Lodkina, I.G., and Yermolaev, M.Yu., Catalog of large-scale solar wind phenomena during 1976–2000, *Cosmic Res.*, 2009, vol. 47, no. 2, pp. 81–94.

30. King, J.H. and Papitashvili, N.E., Solar wind spatial scales in and comparisons of hourly wind and ACE plasma and magnetic field data, *J. Geophys. Res.*, 2004, vol. 110, no. A2, A02209. doi 10.1029/2004JA010804

31. Thatcher, L.J. and Muller, H.-R., Statistical investigation of hourly OMNI solar wind data, *J. Geophys. Res.*, 2011, vol. 116, A12107. doi 10.1029/2011JA017027

32. Mitsakou, E. and Moussas, X., Statistical study of ICMES and their sheaths during solar cycle 23 (1996–2008), *Sol. Phys.*, 2014, vol. 289, pp. 3137–3157. doi 10.1007/s11207-014-0505-y

33. Richardson, I.G. and Cane, H.V., Near-earth solar wind flows and related geomagnetic activity during more than four solar cycles (1963–2011), *J. Space Weather Space Clim.*, 2012, vol. 2, A02. doi 10.1051/swsc/2012003

34. Keesee, A.M., Elfritz, J.G., Fok, M.-C., et al., Superposed epoch analyses of ion temperatures during CME- and CIR/HSS-driven storms, *J. Atmos. Sol.-Terr. Phys.*, 2013, vol. 115, pp. 67–78. doi 10.1016/j.jastp.2013.08.009

35. Potapov, A.S., ULF wave activity in high-speed streams of the solar wind: Impact on the magnetosphere, *J. Geophys. Res.*, 2013, vol. 118, pp. 6465–6477. doi 10.1002/2013JA019119

36. Yuan, C.J. and Zong, Q.G., The double-belt outer radiation belt during CME- and CIR-driven geomagnetic storms, *J. Geophys. Res.*, 2013, vol. 118, pp. 6291–6301. 10.1002/jgra.50564

37. Cramer, W.D., Turner, N.E., Fok, M.-C., and Buzulukova, N.Y., Effects of different geomagnetic storm drivers on the ring current: CRCM results, *J. Geophys. Res.*, 2013, vol. 118, pp. 1062–1073. doi 10.1002/jgra.50138

38. Kim, K.-C., Lee, D.-Y., and Shprits, Y., Dependence of plasmaspheric hiss on solar wind parameters and geomagnetic activity and modeling of its global distribution, *J. Geophys. Res.*, 2015, vol. 120, pp. 1153–1167. doi 10.1002/2014JA020687

39. Yermolaev, Y.I., Nikolaeva, N.S., Lodkina, I.G., and Yermolaev, M.Y., Large-scale solar wind structures: Occurrence rate and geoeffectiveness, *AIP Conf. Proc.*, 2010, vol. 1216, pp. 648–651.

40. Hutchinson, J.A., Wright, D.M., and Milan, S.E., Geomagnetic storms over the last solar cycle: A superposed epoch analysis, *J. Geophys. Res.*, 2011, vol. 116, A09211. doi 10.1029/2011JA016463

41. Zolotukhina, N., Polekh, N., Kurkin, V., and Romanova, E., Ionospheric effects of solar flares and their associated particle ejections in March 2012, *Adv. Space Res.*, 2015, vol. 55, pp. 2851–2862.

42. Yermolaev, Yu.I., Lodkina, I.G., Nikolaeva, N.S., and Yermolaev, M.Yu., Dynamics of large-scale solar-wind streams obtained by the double superposed epoch analysis. 2. CIR vs Sheath and MC vs Ejecta comparisons. 2016. http://arxiv.org/abs/1602.08899.

Translated by Yu. Preobrazhensky